JOURNAL OF GUIDANCE, CONTROL, AND DYNAMICS
Vol. 29, No. 3, May–June 2006

Adaptive Formation Control for Rovers Traveling over Unknown Terrains

Farid Ganji* and Sanjay S. Joshi†
University of California, Davis, California 95616
and
David S. Bayard‡
Jet Propulsion Laboratory, Pasadena, California 91101

A novel adaptive formation-control strategy for a group of rovers navigating over unknown terrain is presented. A leader–follower formation control architecture is employed. Direct adaptive control laws and a formation speed adaptation strategy are developed that 1) bring the rovers into a prescribed formation from arbitrary in-plane locations and 2) enable the group to navigate over unknown and changing terrain, while staying in formation in the presence of actuator saturation. On-line estimates of generic friction parameters account for terrain surface variations. The leader specifies a reference motion for the entire fleet, including both straight-line and turning maneuvers. In saturation events, the formation speed is reduced based on the maximum sustainable speed of the slowest saturated rover using internal fleet communication, allowing the formation error to stay bounded and small. A formal proof for asymptotic stability of the formation system under nonsaturated conditions is given. A simulation example is presented that demonstrates formation initialization, formation-keeping, and formation-switching in both actuator saturation and nonsaturation circumstances.

Nomenclature

c_n	=	follower's adaptive controller feedback gain
$\boldsymbol{E}_{nj}$	=	follower's tracking-error state vector
$\boldsymbol{e}_n$	=	follower's tracking-error vector
e_{nj}	=	follower's scalar tracking-error in inertial directions
F_n	=	rover's control force magnitude
$F_n^{\max}$	=	rover's actuator saturation limit
$\boldsymbol{f}_n$	=	rover's control force per unit mass
g	=	acceleration due to gravity
k_n	=	follower's adaptive controller feedback gain
k_P, k_I	=	leader's PI-controller feedback gains
L	=	formation size
m_n	=	rover's mass
N	=	number of rovers in the fleet
$\boldsymbol{n}_n$	=	unit vector normal to rover's path
p_n	=	follower's parameter-estimation gain
Q_n	=	follower's separation distance (Euclidian or arc)
Q_{nS}, Q_{nN}	=	follower's scalar separations along leader's path-frame axes
$\boldsymbol{q}_n$	=	follower's separation vector from the leader
q_{nX}, q_{nY}	=	follower's scalar separations in inertial directions
$\boldsymbol{r}_n$	=	rover's inertial position vector
$\boldsymbol{s}_n$	=	unit vector tangent to rover's path (rover's heading vector)
t	=	time
$\boldsymbol{u}_n$	=	rover's control-force unit vector
V_n	=	aggregate Lyapunov function
V_{nj}	=	directional Lyapunov function
$\boldsymbol{v}_n$	=	rover's absolute velocity vector
v_n	=	rover's linear speed
v_{nd}	=	rover's desired formation speed
v_{nj}	=	rover's speed in inertial directions
$\bar{v}_{0d}$	=	leader's desired formation speed in saturation events
$\bar{v}_n$	=	rover's saturation speed
x_n, y_n	=	rover's inertial position coordinates
β_n	=	terrain's viscous friction coefficient
$\hat{\beta}_{nj}$, $\tilde{\beta}_{nj}$	=	follower's viscous parameter estimate (of its own terrain), estimation error
$\hat{\beta}_{0nj}$, $\tilde{\beta}_{0nj}$	=	follower's viscous parameter estimate (of leader's terrain), estimation error
$\boldsymbol{\Gamma}_n$	=	gain matrix in Lyapunov function
μ_n	=	terrain's Coulomb friction coefficient
$\hat{\mu}_{nj}$, $\tilde{\mu}_{nj}$	=	follower's Coulomb parameter estimate (of its own terrain), estimation error
$\hat{\mu}_{0nj}$, $\tilde{\mu}_{0nj}$	=	follower's Coulomb parameter estimate (of leader's terrain), estimation error
τ_n	=	rover's saturation-signal delay
ψ_n	=	rover's heading angle in world frame
ψ_{0d}	=	leader's desired heading angle
$\boldsymbol{\omega}_n$	=	rover's angular velocity vector
ω_n	=	rover's turn rate (angular speed)
ω_{0d}	=	leader's desired turn rate
$\bar{\omega}_{0d}$	=	leader's desired turn rate in saturation events

Subscripts

d	=	desired
j	=	inertial direction (X, Y)
n	=	rover index

Received 21 December 2004; revision received 16 September 2005; accepted for publication 19 September 2005.

*Ph.D. Candidate, Department of Mechanical and Aeronautical Engineering. Student Member AIAA.

†Assistant Professor, Department of Mechanical and Aeronautical Engineering; maejoshi@ucdavis.edu. Senior Member AIAA.

‡Senior Research Scientist, Guidance and Control Analysis Group. Senior Member AIAA.

I. Introduction

MANY future planetary exploration missions will incorporate multiple cooperative robots that all work together for maximum scientific return or infrastructure construction. The trend of using multiple robots for planetary exploration began with the Mars Exploration Rover missions, which employed two rovers on the ground at the same time (although not working cooperatively).[1] The advantages of robot teams include the potential to share sensors, the potential to carry long extended objects, the potential to explore large areas simultaneously, and the potential for one robot

to teach other robots.[2–4] However, robot teams for space exploration missions must contend with the unique characteristics of space exploration missions, including the fact that terrain conditions may be unknown and/or distance-varying. Formation-keeping is the ability of each member of a robot team to maintain a desired relative geometry (including position and/or attitude) with respect to a point that moves with the formation as a whole. In this paper, we develop adaptive control laws and navigation strategies for a fleet of point-mass robots, such that the fleet as a whole maintains a certain relative geometric configuration, in the face of unknown and changing terrain conditions, as well as actuator saturation.

In robotic exploration, the terrain conditions that the fleet encounters will not be known for certain and are likely to change over distance traveled. Furthermore, each robot in the formation may experience a different terrain condition. Thus, it will be important to account for robot–terrain interaction effects. On the other hand, actuator saturation is closely linked to terrain difficulty. More difficult terrain demands greater control forces, which may not be available, and hence may end up saturating the robots' actuators. As such, under saturating conditions, individual robot adaptation may not be sufficient for formation maintenance and a higher-level approach may be needed, using follower-to-leader communication for group adaptation.

In the field of autonomous mobile ground robotics, formation generation and formation-keeping have received considerable recent interest (e.g., Refs. 5–7). In addition, similar concepts have been used in the control of formations of spacecraft (e.g., Refs. 8 and 9; for a good overview see Ref. 10), aircraft (e.g., Ref. 11), and underwater vehicles (e.g., Ref. 12). Currently, there are three common approaches for robots (ground, air, space, or sea) to coordinate their control strategies to move in formation: 1) so-called behavior-based approaches, 2) virtual structure approaches, and 3) the leader–following approaches. Behavior-based approaches construct overall controllers by combining the effects of possibly competing task-level actions (e.g., Go to Goal, Avoid Obstacles), as a result of which group dynamics emerge (e.g., Refs. 5–7). A disadvantage of using behavior-based approaches is that the emergent group dynamics is difficult to describe mathematically, which in turn makes it difficult to prescribe formation maneuvers and show stability, or study the effects of robot dynamics and environmental uncertainty on the formation control system performance. Recently, research has been reported that analyzed one behavior-based formation controller in a rigorous mathematical framework.[13] In the virtual structure approach, the entire formation is considered as a single rigid body in which the robots are embedded (e.g., Ref. 14). Movement is then prescribed for the virtual structure as a whole, and the individual robot controls needed to keep the structure intact are derived from the overall structure's motion. This method has the advantage that individual robot motion can easily be prescribed by considering the formation motion. However, the method may be inefficient when the virtual structure may have to change often as mission requirements change. Also, if the virtual structure moves in ways such that physically unachievable demands are placed on the individual robots, the formation will break. A solution to this problem is to add feedback from the individual robots to the virtual structure, as has been described in Refs. 15 and 16. In the leader–follower approach, which we adopt in this study, one robot is designated as the leader and the remaining robots follow the leader's motion offset by a distance. A major advantage of the leader–following approach is that it essentially reduces to a tracking problem (leader-tracking in our study), where stability of the tracking errors can be analyzed through techniques in dynamic systems and control theory (e.g., Refs. 9 and 17–19). Another advantage of the leader-following approach is that formation maneuvers can be specified in terms of the leader's motion. One disadvantage of the leader-following approach is that the leader's motion is independent of the motion of the followers. Therefore, if the leader moves in ways that the followers cannot accommodate, the formation cannot be maintained. To compensate for this apparent lack of robustness, feedback from the followers to the leader may again be added. We explore this issue for formation-keeping under actuator saturation in this paper.

As mentioned previously, we consider uncertainty and distance variation of planetary terrain a key concern for planetary exploration. Thus, in this paper, we examine ground mobile robot formation-keeping in an uncertain environment using adaptive control. Adaptive control ideas have been explored previously for formation flying of spacecraft (e.g., Refs. 20 and 21) and formation flying of aircraft (e.g., Ref. 22). Swaroop et al.[23] considered adaptive control for one-dimensional longitudinal control of automated highway car platoons. This paper is a continuation of our work reported in Refs. 24–26, in which we further study adaptive behavior within a fleet of point-mass mobile robots moving in formation over unknown terrain.

The goal of any formation-keeping is to maintain a specific geometric pattern with respect to some reference point in space moving with the formation. In our case, the moving reference point for each following robot will be the fleet leader. In our formation control architecture, the leader defines the reference motion for the fleet using a proportional integral (PI) velocity controller and a speed regulator. The velocity controller's input commands are the desired formation speed and desired heading angle set by the mission requirements. The speed regulator selects and updates the formation linear and angular speeds based on mission requirements and fleet member saturation. To account for possible terrain-condition uncertainties and changes, the follower robots are equipped with parameter estimators, which are used as part of their adaptive controllers. The parameters to be estimated represent the friction effects of the terrain on the robots' dynamics. As mentioned above, a generic friction model, including both Coulomb and viscous friction parameters, summarizes the terrain surface condition for the robot control system. The Coulomb and viscous friction coefficients may represent rolling resistance (due to wheel–terrain interaction normal force) and sinkage/hydrodynamic drag (due to wheel–terrain interaction shear forces) for off-road land vehicles, respectively. However, as will be seen, the terrain parameters need not converge to their true values for the formation to stay intact.

This paper is organized as follows. In Sec. II, we develop the problem and analytical framework. In Sec. III, we define the notion of a robot formation. In Sec. IV, we develop the control and estimation solution via adaptive control. In Sec. V, we prove asymptotic stability of the formation under nonsaturated conditions using the controllers and estimators developed previously. In Sec. VI, we discuss formation motion planning, actuator saturation, and communication protocols. In Sec. VII, we describe a detailed two-dimensional simulation example of a three-robot formation dealing with unknown and changing terrain, actuator saturation, formation transitions, and obstacle avoidance. Finally, in Sec. VIII, we conclude.

II. Problem Formulation

A. Coordinate Systems and Robot Kinematics

Consider N autonomous point-mass mobile robots traveling in a group that desire to keep a formation pattern in the horizontal plane (XY plane) of an inertial world frame (XYZ coordinates), defined with a fixed orthonormal basis $(\boldsymbol{i}, \boldsymbol{j}, \boldsymbol{k})$. The robots' common knowledge of the orientation of inertial axes is assumed to be provided by the sensory data. Each robot is represented by a point mass whose position in the horizontal plane is represented by $\boldsymbol{r}_n = x_n\boldsymbol{i} + y_n\boldsymbol{j}$, where $n \in \{0, 1, \ldots, N-1\}$ (index 0 identifies the leader robot). Initially, the robots are at rest in arbitrary positions, that is, not necessarily in formation. Define a path frame with orthonormal bases $(\boldsymbol{s}_n, \boldsymbol{n}_n, \boldsymbol{k})$ for each rover as follows. First, denote robot n's in-plane linear velocity vector by $\boldsymbol{v}_n$ as

$$\boldsymbol{v}_n = \dot{\boldsymbol{r}}_n = v_{nX}\boldsymbol{i} + v_{nY}\boldsymbol{j} = v_n\boldsymbol{s}_n \tag{1}$$

and by taking $\boldsymbol{k}$ as the unit vector normal to the XY plane,

$$\boldsymbol{n}_n = \boldsymbol{k} \times \boldsymbol{s}_n \tag{2}$$

where v_n is nonnegative. The overdot denotes vector differentiation with respect to time in the inertial frame; it will be used in the rest of this text. Based on these definitions, at each point along robot n's

path, $\boldsymbol{s}_n$ (heading vector) is the unit vector tangent to the path in the direction of the robot's velocity, and $\boldsymbol{n}_n$ is the unit vector normal to the path as defined above. Denoting robot n's heading angle in the world frame by ψ_n,

$$\boldsymbol{s}_n = \cos\psi_n \boldsymbol{i} + \sin\psi_n \boldsymbol{j} \tag{3}$$

$$\boldsymbol{n}_n = -\sin\psi_n \boldsymbol{i} + \cos\psi_n \boldsymbol{j} \tag{4}$$

Robot n's heading angle ψ_n is related to its inertial speeds as follows:

$$\psi_n = \text{atan2}(v_{nX}, v_{nY}) \tag{5}$$

where atan2 is the four-quadrant inverse tangent function. Also, denoting robot n's angular velocity by $\boldsymbol{\omega}_n$,

$$\boldsymbol{\omega}_n = \dot{\psi}_n \boldsymbol{k} = \omega_n \boldsymbol{k} \tag{6}$$

As will be seen in the next section, the desired heading angles and angular speeds must be available to the rovers, because they will appear in our proposed control laws. Finally, based on these definitions, robot n's acceleration can be written as follows:

$$\ddot{\boldsymbol{r}}_n = \dot{\boldsymbol{v}}_n = \dot{v}_n \boldsymbol{s}_n + \omega_n v_n \boldsymbol{n}_n \tag{7}$$

where the first and second terms on the right-hand side of Eq. (7) represent its longitudinal and lateral accelerations respectively.

B. Robot Dynamics Model

As previously mentioned, the robots are considered point-masses, whose equations of motion are

$$m_n \ddot{\boldsymbol{r}}_n = \boldsymbol{F}_n^{\text{Control}} + \boldsymbol{F}_n^{\text{Terrain}} \tag{8}$$

where m_n is considered to be known, $\boldsymbol{F}_n^{\text{Control}}$ is the available control force driving the robot, and $\boldsymbol{F}_n^{\text{Terrain}}$ is the sum of all terrain-induced forces on the robot, which will be described in the following section. We consider the case where the available control force is limited, so that the rovers' actuators may saturate in difficult terrain. Therefore, the control force can be described as follows:

$$\boldsymbol{F}_n^{\text{Control}} = F_n \boldsymbol{u}_n = \text{sat}\left\{F_{nd}, F_n^{\max}\right\} \boldsymbol{u}_n \tag{9}$$

where F_n and F_{nd} are the magnitudes (nonnegative) of the actual and desired driving control force, and sat{. , .} is the general saturation function with saturation limit σ as described in Eq. (10):

$$\text{sat}\{w, \sigma\} = \begin{cases} \text{sgn}(w)\sigma & \text{if} \quad |w| \geq \sigma \\ w & \text{if} \quad |w| < \sigma \end{cases} \tag{10}$$

C. Robot–Terrain Interaction Dynamics Model

Detailed models of surface terrain effects on ground rovers include analysis of soil properties, wheel construction, and depth of sinkage.[27,28] For purposes of rover adaptive control design, complex terrain should be represented using a small number of terrain parameters (to limit the complexity of the controllers). Representative terrain-induced forces considered in this design are longitudinal and lateral friction forces in the horizontal plane. We consider the longitudinal force to be composed of Coulomb and viscous friction components opposing the robot's motion[29] and the lateral force to be normal to the direction of motion. The total terrain force acting on robot n can be described as follows:

$$\boldsymbol{F}_n^{\text{Terrain}} = \boldsymbol{F}_n^{\text{Coulomb}} + \boldsymbol{F}_n^{\text{Viscous}} + \boldsymbol{F}_n^{\text{Lateral}} \tag{11}$$

The Coulomb and viscous forces may be described as

$$\boldsymbol{F}_n^{\text{Coulomb}} = -\mu_n m_n g \boldsymbol{s}_n \tag{12}$$

$$\boldsymbol{F}_n^{\text{Viscous}} = -\beta_n m_n g \boldsymbol{v}_n \tag{13}$$

where μ_n and β_n are unknown to the robot. Although decomposed into several physically motivated terms in other complex terrain models, for a given rover and terrain condition, most terrain models can ultimately be written in this functional form.[27,30] In this study, we assume that μ_n and β_n are nonnegative piecewise constants; that is, they vary in a stepwise manner from one zone to another. The required size of the piecewise constant zones depends on the convergence rate of the controllers and the physical speed of the rovers. In our simulations, the zone frictions need to be constant on the order of a few rover lengths, which is realistic for Earth (lake beds, deserts, fields, etc.) and seems to be realistic for other planetary terrains.[1]

The terrain's lateral force makes turning maneuvers possible by providing the centripetal force necessary to maintain the desired steady-state angular velocity of the rover (as long as the lateral acceleration remains below a certain skidding level). The maximum lateral acceleration of a land vehicle supported by a given terrain may be quantified by $\bar{\mu}_S g$, where $\bar{\mu}_S$ is the maximum rover–terrain static sliding-friction coefficient. Therefore,

$$\boldsymbol{F}_n^{\text{Lateral}} = m_n \text{sat}\{\omega_n v_n, \bar{\mu}_{Sn} g\} \boldsymbol{n}_n \tag{14}$$

It should be noted that although $\bar{\mu}_{Sn}$ is also unknown to the robots, skidding is not a practical concern, considering that planetary rovers are typically low-power vehicles capable of performing low-speed and hence low-lateral-acceleration maneuvers. As such, in this paper we assume a terrain lateral force as

$$\boldsymbol{F}_n^{\text{Lateral}} = m_n \omega_n v_n \boldsymbol{n}_n \tag{15}$$

Therefore, substituting Eqs. (12), (13), and (15) into Eq. (11), we can write the combined terrain force as

$$\boldsymbol{F}_n^{\text{Terrain}} = -(\mu_n + \beta_n v_n) m_n g \boldsymbol{s}_n + m_n \omega_n v_n \boldsymbol{n}_n \tag{16}$$

Finally, substituting from Eq. (16) into Eq. (8), the robot–terrain interaction model takes the form

$$m_n \ddot{\boldsymbol{r}}_n = \boldsymbol{F}_n^{\text{Control}} - (\mu_n + \beta_n v_n) m_n g \boldsymbol{s}_n + m_n \omega_n v_n \boldsymbol{n}_n \tag{17}$$

Dividing Eq. (17) by robot n's known mass m_n yields

$$\ddot{\boldsymbol{r}}_n = \boldsymbol{f}_n - (\mu_n + \beta_n v_n) g \boldsymbol{s}_n + \omega_n v_n \boldsymbol{n}_n \tag{18}$$

where

$$\boldsymbol{f}_n = (1/m_n) \boldsymbol{F}_n^{\text{Control}} \tag{19}$$

For the leader robot, Eq. (18) can also be written in first-order form as

$$\dot{\boldsymbol{v}}_0 = \boldsymbol{f}_0 - (\mu_0 + \beta_0 v_0) g \boldsymbol{s}_0 + \omega_0 v_0 \boldsymbol{n}_0 \tag{20}$$

which will be the governing equation of motion in designing the leader's PI velocity controller to drive the leader's linear speed, heading angle, and angular speed toward the mission-desired values.

III. Robot Formations

Let the leader robot ($n = 0$) be designated as the reference robot for the rest of the fleet ($n = 1$ to $N - 1$). The goal of any formation-keeping is to maintain a specific geometric pattern with respect to some reference point in space that moves with the formation. In our case, the moving reference point for each following robot will be the fleet leader. Let us denote robot n's desired position and velocity vectors in the world frame by $\boldsymbol{r}_{nd}$ and $\boldsymbol{v}_{nd}$, respectively. Therefore,

$$\boldsymbol{r}_{nd} = \boldsymbol{r}_0 + \boldsymbol{q}_n \tag{21}$$

$$\boldsymbol{v}_{nd} = v_{nd} \boldsymbol{s}_{nd} = \boldsymbol{v}_0 + \dot{\boldsymbol{q}}_n \tag{22}$$

where $\boldsymbol{q}_n$ will be described in the next section. In Eq. (22), v_{nd} and $\boldsymbol{s}_{nd}$ denote robot n's desired speed and heading vector during formation navigation, respectively. In what follows, we define various formation patterns by specifying their corresponding separation vectors.

We consider a formation to be rigid when its geometric configuration is preserved during navigation. Some examples of rigid formations are line-abreast (or line), column, arrow, and circular

patterns. Considering the previous definition of the leader's path frame, the general separation vector for the follower robot n in a rigid formation can be defined as follows:

$$\boldsymbol{q}_n^{\text{General}} = -Q_{nN}\boldsymbol{n}_0 - Q_{nS}\boldsymbol{s}_0 = q_{nX}\boldsymbol{i} + q_{nY}\boldsymbol{j} \tag{23}$$

where Q_{nN} and Q_{nS} are defined as positive when a follower's desired position lies to the right and/or behind the leader, respectively. In Eq. (23), q_{nX} and q_{nY} represent separation distances along the inertial axes. For the case of line and column formation patterns, from Eq. (23),

$$\boldsymbol{q}_n^{\text{Line}} = -Q_{nN}\boldsymbol{n}_0 \tag{24}$$

$$\boldsymbol{q}_n^{\text{Column}} = -Q_{nS}\boldsymbol{s}_0 \tag{25}$$

The current work also allows flexible formations in a leader-following control architecture, where the formation geometry changes during certain navigational maneuvers. For example, we may achieve convoy motion in which the follower robots tailgate the leader by some desired distance, while negotiating obstacles using straight lines and circular arcs.[30] Sample results are presented in Sec. VII.

IV. Formation Control

A. Leader Robot's PI Velocity Controller

Define the leader's desired velocity $\boldsymbol{v}_{0d}$ as

$$\boldsymbol{v}_{0d} = v_{0d}\boldsymbol{s}_{0d} \tag{26}$$

where v_{0d} denotes the constant desired speed of the leader during straight-line or turning maneuvers, and $\boldsymbol{s}_{0d}$ represents the corresponding desired-heading vector. In the inertial frame

$$\boldsymbol{s}_{0d} = \cos\psi_{0d}\boldsymbol{i} + \sin\psi_{0d}\boldsymbol{j} \tag{27}$$

where ψ_{0d} is the desired heading of the leader during the maneuver. Denoting the desired straight-line (preturn) constant heading angle by $\psi_{0d}^{\text{preturn}}$, the subsequent desired in-turn heading angle is given by

$$\psi_{0d}^{\text{in-turn}} = \psi_{0d}^{\text{preturn}} + \omega_{0d}\left(t - t_0^{\text{turn}}\right) \tag{28}$$

where t_0^{turn} is the time when turning begins, and ω_{0d} is the constant desired-turning-rate. With $\boldsymbol{v}_{0d}$ as described above, the desired control force computed by the leader's PI velocity controller is given by

$$\boldsymbol{f}_{0d} = f_{0d}\boldsymbol{u}_0 = k_P(\boldsymbol{v}_{0d} - \boldsymbol{v}_0) + k_I\int(\boldsymbol{v}_{0d} - \boldsymbol{v}_0)\,\mathrm{d}t \tag{29}$$

The desired leader control force is subject to actuator saturation and, thus, the available control force to drive the leader is given in Eq. (30) (see Eq. (9) and Eq. (19)):

$$\boldsymbol{F}_0^{\text{Control}} = \text{sat}\left\{m_0 f_{0d},\, F_0^{\max}\right\}\boldsymbol{u}_0 = F_0\boldsymbol{u}_0 = m_0\boldsymbol{f}_0 \tag{30}$$

B. Follower Robots' Tracking-Error Dynamics

The tracking error $\boldsymbol{e}_n$ between the desired and the actual position of the follower robot n along its path is

$$\boldsymbol{e}_n = \boldsymbol{r}_{nd} - \boldsymbol{r}_n \tag{31}$$

Using Eq. (21), we obtain

$$\boldsymbol{e}_n = \boldsymbol{r}_0 - \boldsymbol{r}_n + \boldsymbol{q}_n \tag{32}$$

Differentiating Eq. (32) once and twice, respectively, yields

$$\dot{\boldsymbol{e}}_n = \dot{\boldsymbol{r}}_0 - \dot{\boldsymbol{r}}_n + \dot{\boldsymbol{q}}_n = \boldsymbol{v}_0 - \boldsymbol{v}_n + \dot{\boldsymbol{q}}_n \tag{33}$$

$$\ddot{\boldsymbol{e}}_n = \ddot{\boldsymbol{r}}_0 - \ddot{\boldsymbol{r}}_n + \ddot{\boldsymbol{q}}_n \tag{34}$$

Finally, by substituting from Eq. (18) for $\ddot{\boldsymbol{r}}_0$ and $\ddot{\boldsymbol{r}}_n$ into Eq. (34), the dynamic evolution of tracking errors for the follower robots becomes

$$\ddot{\boldsymbol{e}}_n = \boldsymbol{f}_0 - \boldsymbol{f}_n + (\mu_n\boldsymbol{s}_n - \mu_0\boldsymbol{s}_0 + \beta_n\boldsymbol{v}_n - \beta_0\boldsymbol{v}_0)g + \omega_0 v_0\boldsymbol{n}_0 - \omega_n v_n\boldsymbol{n}_n + \ddot{\boldsymbol{q}}_n \tag{35}$$

Because the goal of formation control is to keep tracking control errors $\boldsymbol{e}_1$ through $\boldsymbol{e}_{N-1}$ as small as possible (and ideally zero) over time, Eq. (35) may be used to motivate controllers that drive the tracking errors to zero.[17] Note that in reality, a priori knowledge of the friction coefficients μ_n, μ_0, β_n, and β_0 present in Eq. (35) is not available. The terrain may also change and/or may be unknown, as in the case of planetary rovers on other planets.[6] In the following, we develop a direct adaptive controller that deals with these terrain uncertainties. Note that we assume level terrain (no slopes) whose frictional characteristics may only vary from one zone to another in a stepwise manner (terrain friction coefficients piecewise constant).

C. Formation Error

Define a nondimensional overall formation error as

$$\boldsymbol{e}_{\text{formation}} = \frac{1}{L}\sum_{n=1}^{N-1}|\boldsymbol{e}_n| = \frac{1}{L}\sum_{n=1}^{N-1}\sqrt{\boldsymbol{e}_{nX}^2 + \boldsymbol{e}_{nY}^2} \tag{36}$$

where

$$L = \max\{Q_1, \ldots, Q_{N-1}\} \tag{37}$$

is a measure of the formation size. In Eq. (37), $Q_1, \ldots, Q_{N-1}$ represent the desired scalar separations (Euclidean or arc) between the leader and the follower robots. It this paper, Q_n are constants that are changed in a stepwise manner during navigation when the mission plan warrants, whereas $\boldsymbol{q}_n$ are the corresponding separation vectors which vary in a continuous manner in the inertial frame during turning maneuvers (e.g., they undergo sinusoidal variation in circular turns).

D. Direct Adaptive Formation Control

By considering the form of Eq. (35) and assuming no a priori knowledge of the terrain friction coefficients μ_n, μ_0, β_n, and β_0, we propose the following direct adaptive formation control laws in vector form for two-dimensional motion of the follower robots ($n = 1$ to $N-1$):

$$\boldsymbol{f}_{nd} = f_{nd}\boldsymbol{u}_n = \boldsymbol{f}_0 + (\hat{\boldsymbol{M}}_n\boldsymbol{s}_n - \hat{\boldsymbol{M}}_{0n}\boldsymbol{s}_0 + \hat{\boldsymbol{B}}_n\boldsymbol{v}_n - \hat{\boldsymbol{B}}_{0n}\boldsymbol{v}_0)g + \omega_0 v_0\boldsymbol{n}_0 - \omega_n v_n\boldsymbol{n}_n + \ddot{\boldsymbol{q}}_n + c_n\dot{\boldsymbol{e}}_n + k_n\boldsymbol{e}_n \tag{38}$$

where the corresponding control force provided by the actuators to drive the follower robots is given by

$$\boldsymbol{F}_n^{\text{Control}} = \text{sat}\left\{m_n f_{nd},\, F_n^{\max}\right\}\boldsymbol{u}_n = F_n\boldsymbol{u}_n = m_n\boldsymbol{f}_n \tag{39}$$

In Eqs. (38) and (39), g, m_n, and $F_n^{\max}$ are known quantities, k_n and c_n are arbitrary positive constant proportional and derivative control gains, respectively, and

$$\hat{\boldsymbol{M}}_n = \begin{bmatrix}\hat{\mu}_{nX} & 0\\ 0 & \hat{\mu}_{nY}\end{bmatrix} \qquad \hat{\boldsymbol{M}}_{0n} = \begin{bmatrix}\hat{\mu}_{0nX} & 0\\ 0 & \hat{\mu}_{0nY}\end{bmatrix}$$

$$\hat{\boldsymbol{B}}_n = \begin{bmatrix}\hat{\beta}_{nX} & 0\\ 0 & \hat{\beta}_{nY}\end{bmatrix} \qquad \hat{\boldsymbol{B}}_{0n} = \begin{bmatrix}\hat{\beta}_{0nX} & 0\\ 0 & \hat{\beta}_{0nY}\end{bmatrix} \tag{40}$$

In Eq. (40), $\hat{\mu}_{nj}$, $\hat{\mu}_{0nj}$, $\hat{\beta}_{nj}$, and $\hat{\beta}_{0nj}$ (where $j = X, Y$) denote follower robot n's time-varying estimates of μ_n, μ_0, β_n, and β_0 in direction j, respectively, updated by their corresponding parameter estimators. Note that the follower robots need to estimate the scalar frictional parameters in each Cartesian direction separately. This requirement will be clarified as we introduce the parameter estimation

law in the next section. At this point, let us also define the estimation error variables in matrix form using Eq. (40) as

$$\tilde{\boldsymbol{M}}_n = \mu_n \boldsymbol{I}_2 - \hat{\boldsymbol{M}}_n \tag{41}$$

$$\tilde{\boldsymbol{M}}_{0n} = \mu_0 \boldsymbol{I}_2 - \hat{\boldsymbol{M}}_{0n} \tag{42}$$

$$\tilde{\boldsymbol{B}}_n = \beta_n \boldsymbol{I}_2 - \hat{\boldsymbol{B}}_n \tag{43}$$

$$\tilde{\boldsymbol{B}}_{0n} = \beta_0 \boldsymbol{I}_2 - \hat{\boldsymbol{B}}_{0n} \tag{44}$$

where $\boldsymbol{I}_2$ is the 2×2 identity matrix.

Notice that for the above controller [Eq. (38)], information regarding $\boldsymbol{f}_0, \boldsymbol{v}_0, \boldsymbol{s}_0, \boldsymbol{n}_0, \omega_0, \ddot{\boldsymbol{q}}_n, \boldsymbol{v}_n, \boldsymbol{s}_n, \boldsymbol{n}_n, \boldsymbol{e}_n$, and $\dot{\boldsymbol{e}}_n$, is assumed to be available via continuous transmission of the required data by the fleet leader to the follower robots, along with the followers' local sensory information.

E. Adaptive Parameter Estimators

In conjunction with the proposed direct adaptive control law in Eq. (38), the scalar frictional parameter estimates in Eq. (40) are updated by the following adaptation laws, as justified in the next section:

$$\dot{\hat{\mu}}_{nX} = [\dot{e}_{nX} + p_n e_{nX}] \cos\psi_n \qquad \dot{\hat{\mu}}_{nY} = [\dot{e}_{nY} + p_n e_{nY}] \sin\psi_n \tag{45}$$

$$\dot{\hat{\mu}}_{0nX} = -[\dot{e}_{nX} + p_n e_{nX}] \cos\psi_0 \qquad \dot{\hat{\mu}}_{0nY} = -[\dot{e}_{nY} + p_n e_{nY}] \sin\psi_0 \tag{46}$$

$$\dot{\hat{\beta}}_{nX} = [\dot{e}_{nX} + p_n e_{nX}] v_{nX} \qquad \dot{\hat{\beta}}_{nY} = [\dot{e}_{nY} + p_n e_{nY}] v_{nY} \tag{47}$$

$$\dot{\hat{\beta}}_{0nX} = -[\dot{e}_{nX} + p_n e_{nX}] v_{0X} \qquad \dot{\hat{\beta}}_{0nY} = -[\dot{e}_{nY} + p_n e_{nY}] v_{0Y} \tag{48}$$

where the constant estimation gains p_n are such that

$$0 < p_n < c_n \tag{49}$$

As will be proved in the following section, the gain condition in Eq. (49), along with $k_n > 0$ and $c_n > 0$, is a sufficient condition for asymptotic stability of the formation system when the followers' actuators are not saturated.

V. Formation Stability Analysis Using Lyapunov's Direct Method and Barbalat's Lemma

A. Theorem 1

Let Robots 1 through $N-1$ use the nonsaturated adaptive controllers represented by Eq. (38) and the nonsaturated case of Eq. (39) with arbitrary proportional and derivative feedback control gains $k_n > 0$, $c_n > 0$, and the estimators given in Eqs. (45–48) subject to the estimation-gain condition given in Eq. (49) in order to maintain formation over terrain areas with piecewise constant friction coefficients μ_n and β_n; then the formation pattern is asymptotically stable, so that, for $n = 1$ to $N-1$, $\boldsymbol{e}_n \to \boldsymbol{0}$, and $\dot{\boldsymbol{e}}_n \to \boldsymbol{0}$ as $t \to \infty$.

B. Proof Strategy

Introducing an aggregate Lyapunov function candidate V_n for robot n's error system dynamics, the strategy of the proof is to use Barbalat's lemma to show $\dot{V}_n \to 0$ as $t \to \infty$, where

$$V_n = \sum_j V_{nj}$$

and $j = X, Y$ for two-dimensional motion in the inertial Cartesian frame. Consequently, $\dot{V}_n \to 0$ will explicitly imply $\boldsymbol{e}_n \to \boldsymbol{0}$, and $\dot{\boldsymbol{e}}_n \to \boldsymbol{0}$ as $t \to \infty$, showing the formation pattern is asymptotically stable.

C. Lyapunov-Like Lemma (An Immediate Corollary of Barbalat's Lemma)[31]

If a scalar function $V(\boldsymbol{x}, t)$ satisfies the conditions 1) $V(\boldsymbol{x}, t)$ is lower bounded, 2) $\dot{V}(\boldsymbol{x}, t)$ is negative semidefinite, 3) $\dot{V}(\boldsymbol{x}, t)$ is uniformly continuous in time, then $\dot{V}(\boldsymbol{x}, t) \to 0$ as $t \to \infty$.

For our error dynamics system, the error state vector $\boldsymbol{x}$ can be defined as follows:

$$\boldsymbol{x} = \boldsymbol{x}_{nj} = [e_{nj} \quad \dot{e}_{nj} \quad \tilde{\mu}_{nj} \quad \tilde{\mu}_{0nj} \quad \tilde{\beta}_{nj} \quad \tilde{\beta}_{0nj}]^T \in \Re^6 \tag{50}$$

where $\tilde{\mu}_{nj}, \tilde{\mu}_{0nj}, \tilde{\beta}_{nj}$, and $\tilde{\beta}_{0nj}$ are the diagonal elements of estimation error matrices $\tilde{\boldsymbol{M}}_n, \tilde{\boldsymbol{M}}_{0n}, \tilde{\boldsymbol{B}}_n$, and $\tilde{\boldsymbol{B}}_{0n}$ respectively [Eqs. (41–44)]. Because we have assumed that the controllers of follower robots 1 through $N-1$ are not saturated, from Eqs. (38) and (39),

$$\boldsymbol{f}_n = \boldsymbol{f}_{nd} \qquad n = 1, \ldots, N-1 \tag{51}$$

Therefore, by substituting from Eq. (38) into Eq. (35), the formation tracking-error dynamics will be

$$\ddot{\boldsymbol{e}}_n + c_n \dot{\boldsymbol{e}}_n + k_n \boldsymbol{e}_n = (\tilde{\boldsymbol{M}}_n \boldsymbol{s}_n - \tilde{\boldsymbol{M}}_{0n} \boldsymbol{s}_0 + \tilde{\boldsymbol{B}}_n \boldsymbol{v}_n - \tilde{\boldsymbol{B}}_{0n} \boldsymbol{v}_0) g \tag{52}$$

Now define a directional tracking-error state vector for robot n as

$$\boldsymbol{E}_{nj} = [e_{nj} \quad \dot{e}_{nj}]^T \tag{53}$$

and choose Lyapunov functions in each direction as

$$V_{nj} = \tfrac{1}{2} \boldsymbol{E}_{nj}^T \boldsymbol{\Gamma}_n \boldsymbol{E}_{nj} + \tfrac{1}{2} g \left(\tilde{\mu}_{nj}^2 + \tilde{\mu}_{0nj}^2 + \tilde{\beta}_{nj}^2 + \tilde{\beta}_{0nj}^2 \right) \tag{54}$$

where

$$\boldsymbol{\Gamma}_n = \begin{bmatrix} k_n + p_n c_n & p_n \\ p_n & 1 \end{bmatrix} \tag{55}$$

Imposing the conditions $k_n > 0$, $c_n > 0$, and $0 < p_n \le c_n$ guarantees the gain matrix $\boldsymbol{\Gamma}_n$ to be a positive definite matrix (Sylvester's theorem) and V_n to be a positive definite function, which in turn implies that V_n is lower-bounded (by zero) as required in Condition 1 of the lemma. Differentiating Eq. (54) with respect to time along the controlled error-system trajectory governed by Eq. (52), for $j = X$ and Y, we obtain

$$\begin{aligned} \dot{V}_{nX} = {} & -(c_n - p_n)\dot{e}_{nX}^2 - k_n p_n e_{nX}^2 \\ & + \tilde{\beta}_{nX}\{\dot{\tilde{\beta}}_{nX} + [\dot{e}_{nX} + p_n e_{nX}] v_n \cos\psi_n\} g \\ & + \tilde{\beta}_{0nX}\{\dot{\tilde{\beta}}_{0nX} - [\dot{e}_{nX} + p_n e_{nX}] v_0 \cos\psi_0\} g \\ & + \tilde{\mu}_{nX}\{\dot{\tilde{\mu}}_{nX} + [\dot{e}_{nX} + p_n e_{nX}] \cos\psi_n\} g \\ & + \tilde{\mu}_{0nX}\{\dot{\tilde{\mu}}_{0nX} - [\dot{e}_{nX} + p_n e_{nX}] \cos\psi_0\} g \end{aligned} \tag{56}$$

and

$$\begin{aligned} \dot{V}_{nY} = {} & -(c_n - p_n)\dot{e}_{nY}^2 - k_n p_n e_{nY}^2 \\ & + \tilde{\beta}_{nY}\{\dot{\tilde{\beta}}_{nY} + [\dot{e}_{nY} + p_n e_{nY}] v_n \sin\psi_n\} g \\ & + \tilde{\beta}_{0nY}\{\dot{\tilde{\beta}}_{0nY} - [\dot{e}_{nY} + p_n e_{nY}] v_0 \sin\psi_0\} g \\ & + \tilde{\mu}_{nY}\{\dot{\tilde{\mu}}_{nY} + [\dot{e}_{nY} + p_n e_{nY}] \sin\psi_n\} g \\ & + \tilde{\mu}_{0nY}\{\dot{\tilde{\mu}}_{0nY} - [\dot{e}_{nY} + p_n e_{nY}] \sin\psi_0\} g \end{aligned} \tag{57}$$

Now, because μ_n and β_n are assumed to be piecewise constant, $\dot{\mu}_n = 0$ and $\dot{\beta}_n = 0$. Hence, by differentiating Eqs. (41–44) with respect to time, $\dot{\tilde{\mu}}_{nj} = -\dot{\hat{\mu}}_{nj}$, $\dot{\tilde{\mu}}_{0nj} = -\dot{\hat{\mu}}_{0nj}$, $\dot{\tilde{\beta}}_{nj} = -\dot{\hat{\beta}}_{nj}$, and $\dot{\tilde{\beta}}_{0nj} = -\dot{\hat{\beta}}_{0nj}$. Using these relations in Eqs. (56) and (57) and then substituting for $\dot{\hat{\mu}}_{nj}$, $\dot{\hat{\mu}}_{0nj}$, $\dot{\hat{\beta}}_{nj}$, and $\dot{\hat{\beta}}_{0nj}$ from Eqs. (45–48),

$$\dot{V}_{nj} = -(c_n - p_n)\dot{e}_{nj}^2 - k_n p_n e_{nj}^2 \tag{58}$$

Finally, the conditions $k_n > 0$, $c_n > 0$, along with the stricter condition of $0 < p_n < c_n$, which justifies the gain condition in Eq. (49), imply that $\dot{V}_{nj} \leq 0$ and therefore

$$\dot{V}_n = \sum_j \dot{V}_{nj} = -(c_n - p_n)|\dot{\boldsymbol{e}}_n|^2 - k_n p_n |\boldsymbol{e}_n|^2 \leq 0 \tag{59}$$

which in turn implies Condition 2 of the lemma. To show that $\dot{V}_{nj}$ and hence $\dot{V}_n$ are uniformly continuous, we prove the boundedness of $\ddot{V}_n$, by showing $|\ddot{V}_n| < \infty$ (a sufficient condition for uniform continuity of $\dot{V}_n$). By differentiating $\dot{V}_{nj}$ in Eq. (58) with respect to time to get $\ddot{V}_{nj}$, it is easy to show that

$$|\ddot{V}_{nj}| \leq 2(c_n - p_n)|\dot{e}_{nj}\|\ddot{e}_{nj}| + 2k_n p_n |e_{nj}\|\dot{e}_{nj}| \tag{60}$$

On the other hand, the proved conditions of $V_n > 0$ and $\dot{V}_n \leq 0$ imply that the quantities $|e_{nj}|$, $|\dot{e}_{nj}|$, $|\tilde{\mu}_{nj}|$, $|\tilde{\mu}_{0nj}|$, $|\tilde{\beta}_{nj}|$, and $|\tilde{\beta}_{0nj}|$ are bounded. Now, from Eq. (52), the tracking error dynamics in scalar form are

$$\ddot{e}_{nX} = -c_n \dot{e}_{nX} - k_n e_{nX} + (\tilde{\mu}_{nX} \cos\psi_n - \tilde{\mu}_{0nX} \cos\psi_0 + \tilde{\beta}_{nX} v_n \cos\psi_n - \tilde{\beta}_{0nX} v_0 \cos\psi_0) g \tag{61}$$

$$\ddot{e}_{nY} = -c_n \dot{e}_{nY} - k_n e_{nY} + (\tilde{\mu}_{nY} \sin\psi_n - \tilde{\mu}_{0nY} \sin\psi_0 + \tilde{\beta}_{nY} v_n \sin\psi_n - \tilde{\beta}_{0nY} v_0 \sin\psi_0) g \tag{62}$$

In Eqs. (61) and (62), we have $0 \leq |\cos\psi_n|, |\cos\psi_0|, |\sin\psi_n|, |\sin\psi_0| \leq 1$. Also, we have $0 \leq v_0 < \infty$ and $|\omega_0| < \infty$ due to BIBO stability of the leader's PI controller, which in turn implies that $v_n < \infty$, based on the following proof. From Eq. (33), we obtain

$$\boldsymbol{v}_n = \boldsymbol{v}_0 + \dot{\boldsymbol{q}}_n - \dot{\boldsymbol{e}}_n \tag{63}$$

where the following inequalities hold:

$$|\dot{\boldsymbol{q}}_n| \leq |\omega_0 \| \boldsymbol{q}_n| < \infty \tag{64}$$

$$v_n = |\boldsymbol{v}_n| \leq |\boldsymbol{v}_0| + |\dot{\boldsymbol{q}}_n| + |\dot{\boldsymbol{e}}_n| < \infty \tag{65}$$

Therefore, from Eqs. (61) and (62) we deduce

$$|\ddot{e}_{nj}| \leq c_n |\dot{e}_{nj}| + k_n |e_{nj}| + |\tilde{\mu}_{nj}| g + |\tilde{\mu}_{0nj}| g + |\tilde{\beta}_{nj}| v_n g + |\tilde{\beta}_{0nj}| v_0 g < \infty \tag{66}$$

that leads to $|\ddot{V}_{nj}| < \infty$ from Eq. (60) and consequently

$$|\ddot{V}_n| = \sum_j \ddot{V}_{nj} < \infty$$

which satisfies Condition 3 of the lemma. Finally, since conditions 1, 2, and 3 of the lemma are satisfied for V_n, they imply that $\dot{V}_n \to 0$ as $t \to \infty$, and hence from Eq. (59), we have

$$\dot{V}_n = -(c_n - p_n)|\dot{\boldsymbol{e}}_n|^2 - k_n p_n |\boldsymbol{e}_n|^2 \to 0 \tag{67}$$

which in turn implies that $\boldsymbol{e}_n \to \boldsymbol{0}$ and $\dot{\boldsymbol{e}}_n \to \boldsymbol{0}$ as $t \to \infty$ for the follower robots $n = 1$ to $N - 1$. **QED**.

It is emphasized that the stability results of this theorem are applicable to any choice of proportional and derivative gains $k_n > 0$, $c_n > 0$, since there always exists a corresponding $p_n > 0$ satisfying the gain condition of Eq. (49). We also note that the above proof does not imply that the parameter estimates converge to their true values.

VI. Motion Planning for Formation Navigation

On nonsaturating terrain, the speed and heading-angle/turning rate commands to the leader's PI velocity controller follow their mission-desired values. In the initial get-into-formation (rendezvous) stage, the speed input is set to zero so that out-of-formation robots can move to their expected formation positions. As a result, during the rendezvous period, the leader and in-formation agents, if any, wait in their initial locations while out-of-formation agents 'rush' (may favorably reach their saturation speeds) into their formation positions. In postrendezvous adverse actuator saturation events that tend to break the formation, the leader's desired formation speeds (linear and angular) are reduced following a speed adaptation strategy that will be described in the next section.

A. Speed Adaptation Strategy in Adverse Actuator Saturation Events

In our scheme, in saturation events, the leader reduces the formation speed based on the speed of the slowest saturated robot within the current formation geometry. This prevents the tracking errors from growing (and the formation from breaking) when one or more of the follower robots saturate over difficult terrain. This strategy allows the saturated robots' tracking errors to remain bounded and small. In practice, $\dot{\boldsymbol{e}}_n \to 0$ [Eq. (33)] within two consecutive settling-time periods corresponding to (1) the transient slowdown dynamics of the robot, which runs into the saturating patch, and (2) the leader's speed adjustment response. In our model, the steady-state saturation speeds of the robots in adverse saturation events over difficult terrain are described by

$$0 < \bar{v}_n = \frac{F_n^{\max} - \mu_n m_n g}{\beta_n m_n g} < v_{nd} \tag{68}$$

where $\bar{v}_n$ represents the steady-state saturation speed of robot n over a certain difficult patch and may vary in a stepwise manner from

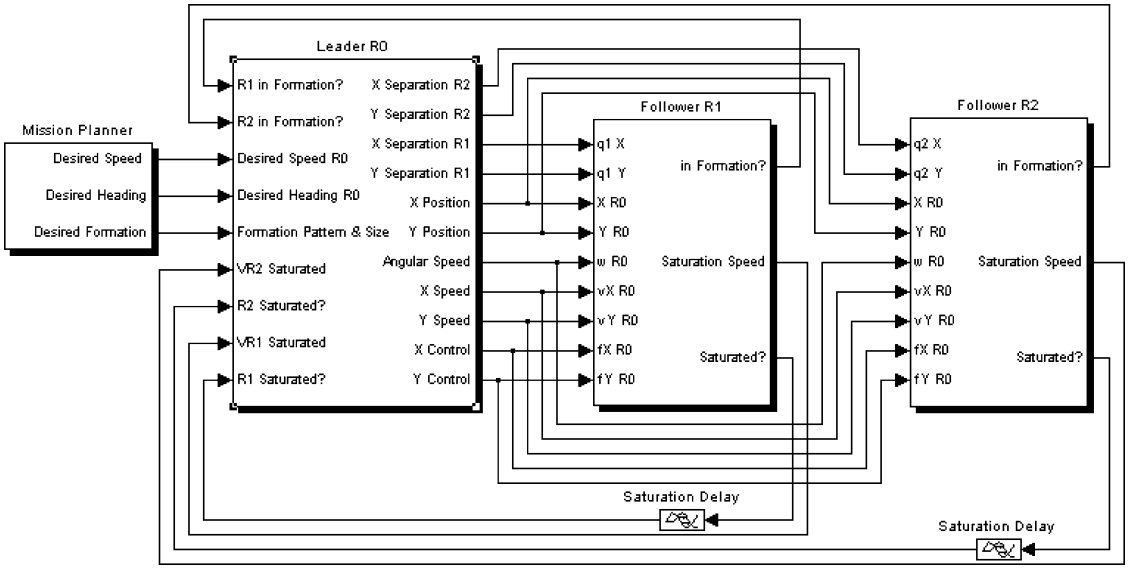

Fig. 1 Top block of our three-robot formation simulator.

one zone to another. In Eq. (68), v_{nd}, which varies in a continuous manner, is the desired speed of robot n within the formation configuration following the leader's instantaneous motion [see Eq. (22)].

It should be noted that there are navigational occasions in which formation-speed adaptation is not needed. One is the "get-into-formation" stage when the leader is at rest and the followers travel toward their formation positions. The other is during commanded switches in formation geometry (when the robots may be saturated and traveling at speeds higher than their desired formation speeds). Also, note that in Eq. (68), $\bar{v}_n \leq 0$ would correspond to an impassible terrain for robot n where the fleet would have to stop. In circumstances where more than one robot is saturated, the leader selects the lowest communicated saturation speed $\bar{v}_n^{\min}$ and reduces the formation speed accordingly. Denoting the leader's adapted speed during saturation events by $\bar{v}_{0d}$, the strategy implies that

$$\bar{v}_{0d} = \bar{v}_n^{\min} \tag{69}$$

Accordingly, to preserve the current path curvature during turning maneuvers (i.e., turning at the same radius) while one or more robots become saturated, the adapted desired angular speed of the leader $\bar{\omega}_{0d}$ is

$$\bar{\omega}_{0d} = \left(\bar{v}_n^{\min} \big/ v_{nd}\right)\omega_{0d} \tag{70}$$

where v_{nd} is the mission-desired nonsaturation linear speed of the most lagging robot, and ω_{0d} is the desired (nonsaturation) formation angular speed [Eq. (28)]. Accordingly, the leader's desired reduced speed will be

$$\bar{v}_{0d} = \sqrt{\bar{v}_n^{\min 2} - (\bar{\omega}_{0d}\, Q_{nS})^2} - \bar{\omega}_{0d}\, Q_{nN} \tag{71}$$

where Q_{nS} and Q_{nN} are the desired scalar separations of the most-lagging robot as described in section ***E***. Following this strategy, other saturated robots with higher speeds ($\bar{v}_n > \bar{v}_n^{\min}$) will unsaturate and hence reach and stay at their desired formation positions with respect to the leader.

The formation-speed adaptation technique is needed for formation-keeping when the follower robots saturate, whereas when the leader runs into a saturating patch, the formation remains in place because the rest of the fleet slows down automatically to track the leader. In our model, to prevent control windup and reduce speed overshoot when robots unsaturate, the adaptive estimators' integral actions are halted during actuator saturation events. In the case of a saturated leader, the speed adaptation acts as an anti-windup mechanism for the leader's PI controller.

B. Communication Protocol

The communication lines and their flow directions between the leader and the rest of the fleet can be seen in Fig. 1. The leader, which is the fleet's motion planner, continuously transmits its state and control information (as well as formation information) to the followers through 11 communication channels. In our simulation model, the information regarding formation separation vectors, as well as the leader's position, linear velocity, and control (force per unit mass) vectors are communicated using inertial components (Fig. 1). In saturation events, followers' saturation information is communicated to the leader using on–off saturated/not-saturated pulses that toggle the signals carrying their saturation speeds. This information is event-triggered and flows through separate channels from each of the followers back to the leader (Fig. 1). As can be seen in Fig. 1, each follower also sends an on–off signal to the leader indicating whether or not it is in its formation position. This signal is only transmitted when an agent is initially out of formation, that is, in the rendezvous stage, and is turned off afterward. In this way, the leader knows if all the robots are in their formation positions before starting the navigation. It is assumed that inertial position and velocity information is available to the robots using appropriate body-mounted sensors.

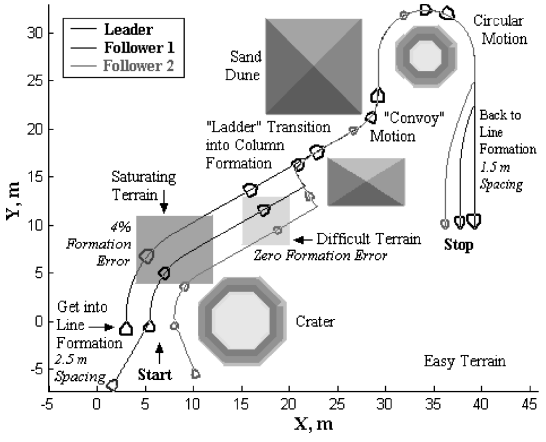

Fig. 2 Traces of the three rovers over unknown terrain. The largest rover is the leader; successively smaller rovers are follower 1 and follower 2.

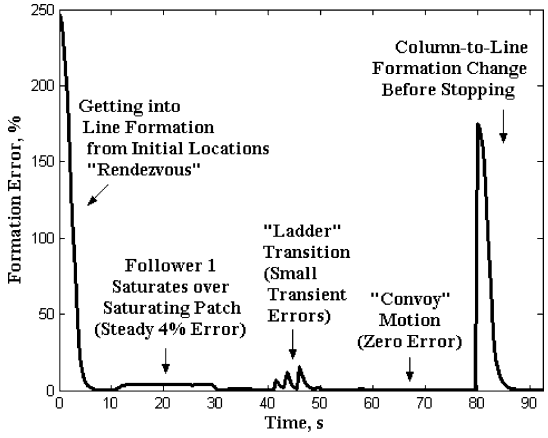

Fig. 4 Percent overall formation error.

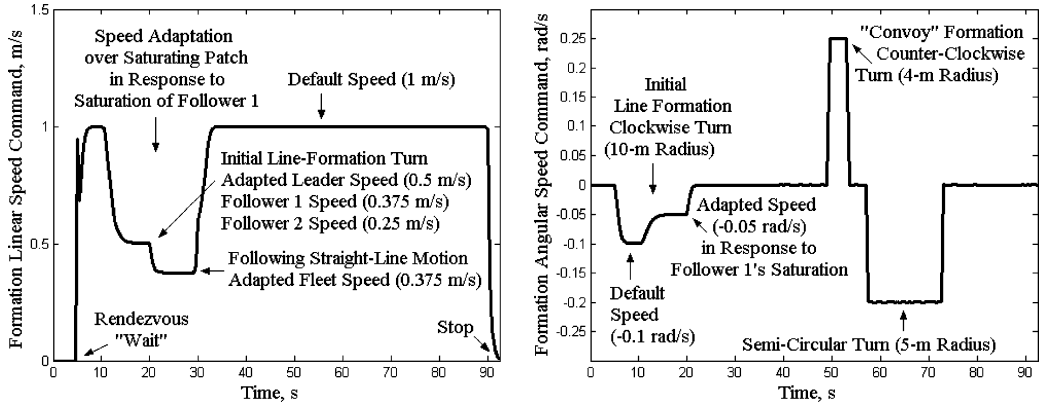

Fig. 3 Leader's formation-speed commands.

In implementing the speed adaptation strategy, we introduced a settling-time delay ("saturation delay") when saturated robots communicate their terrain-dependent saturation speeds to the leader (Fig. 1). In the case of leader saturation, this delay is implemented locally. The reason for imposing this communication delay is to avoid chatter in the leader's formation-speed command, which is set by the speed regulator in response to the saturation signals sent by one or more of the robots in the fleet. The chatter occurs in the form of transient fluctuations between saturation speed and the current default formation speed. With saturation delay in place, the saturated robot settles to its steady-state saturation speed over difficult terrain before communicating its speed to the leader for adaptation purposes.

VII. Simulation Results

For this research, we developed a MATLAB Simulink simulation model for three-robot formations. The top block of the model is shown in Fig. 1. The directed links between the three robot blocks represent continuous, as well as event-triggered, communication lines as described in the previous section. The simulation terrain model is generated in the world frame. In this work, the terrain is simply modeled using Coulomb and viscous friction components. The current terrain model is comprised of rough terrain patches (high friction), obstacles (e.g., sand dunes and craters to be avoided), and large areas of relatively easier terrain (lower friction).

As part of the simulation work, we also implemented two "flexible" formations in the leader-following control architecture, where the formation geometry changes in a desired manner during certain navigational maneuvers. We implemented two types of flexible-formation kinematics in our simulation model—convoy motion and ladder transition. Convoy motion pertains to the case in which the follower robots tailgate the leader by some desired path distance while negotiating circular curves. Practically, convoy motion is beneficial for formation-keeping when the leader moves among obstacles (e.g., using planned or reactive avoidance algorithms). Ladder transition is performed when the followers are commanded to change formation from line to column configuration, in which the followers move laterally across the current line formation while tending to keep a fixed Euclidian distance to the leader.[30]

In what follows, a set of simulation results are presented for a fleet of three mobile robots, with different (known) masses and actuator saturation limits, performing formation navigation

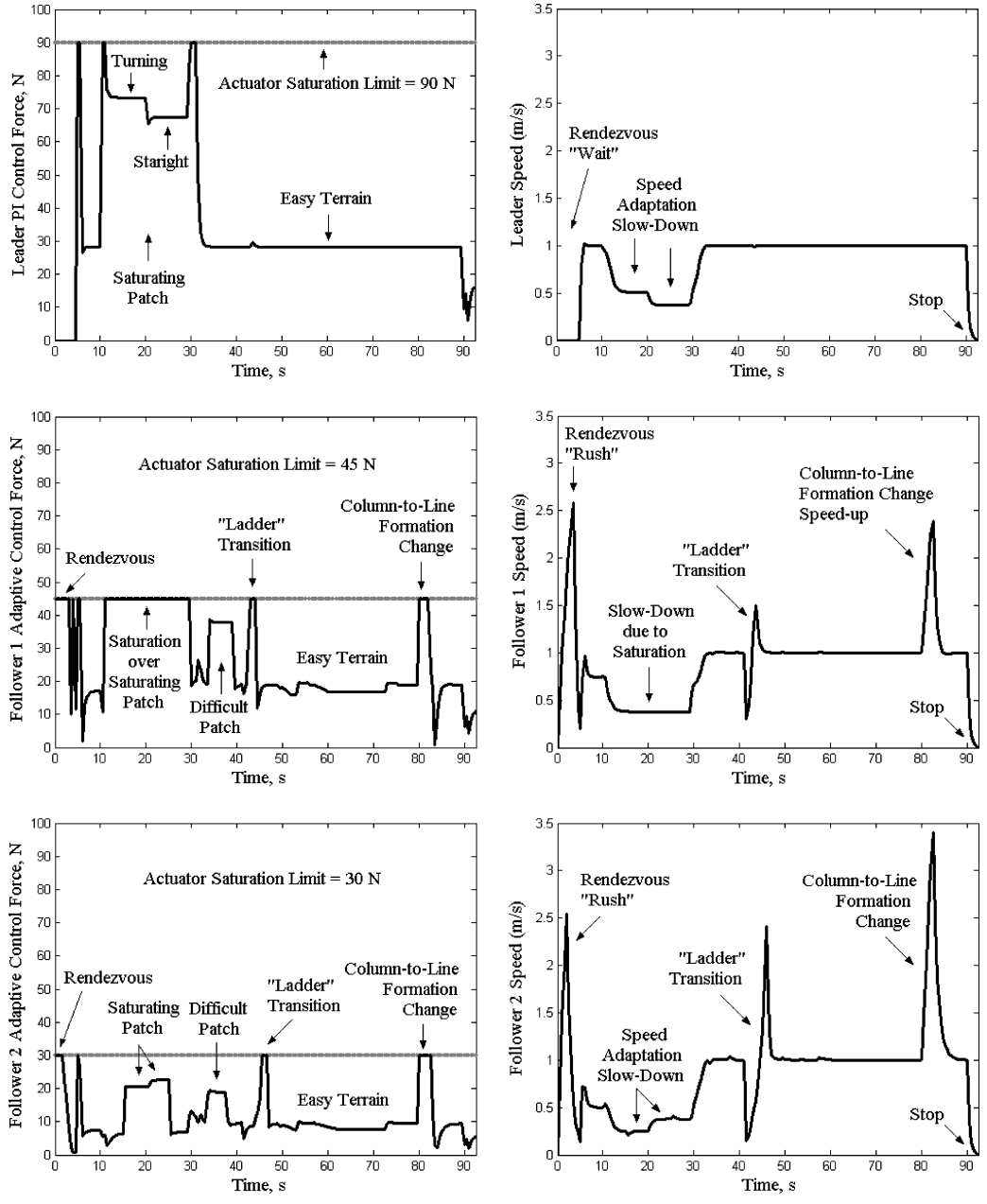

Fig. 5 Rover control force (magnitude) and linear speed histories.

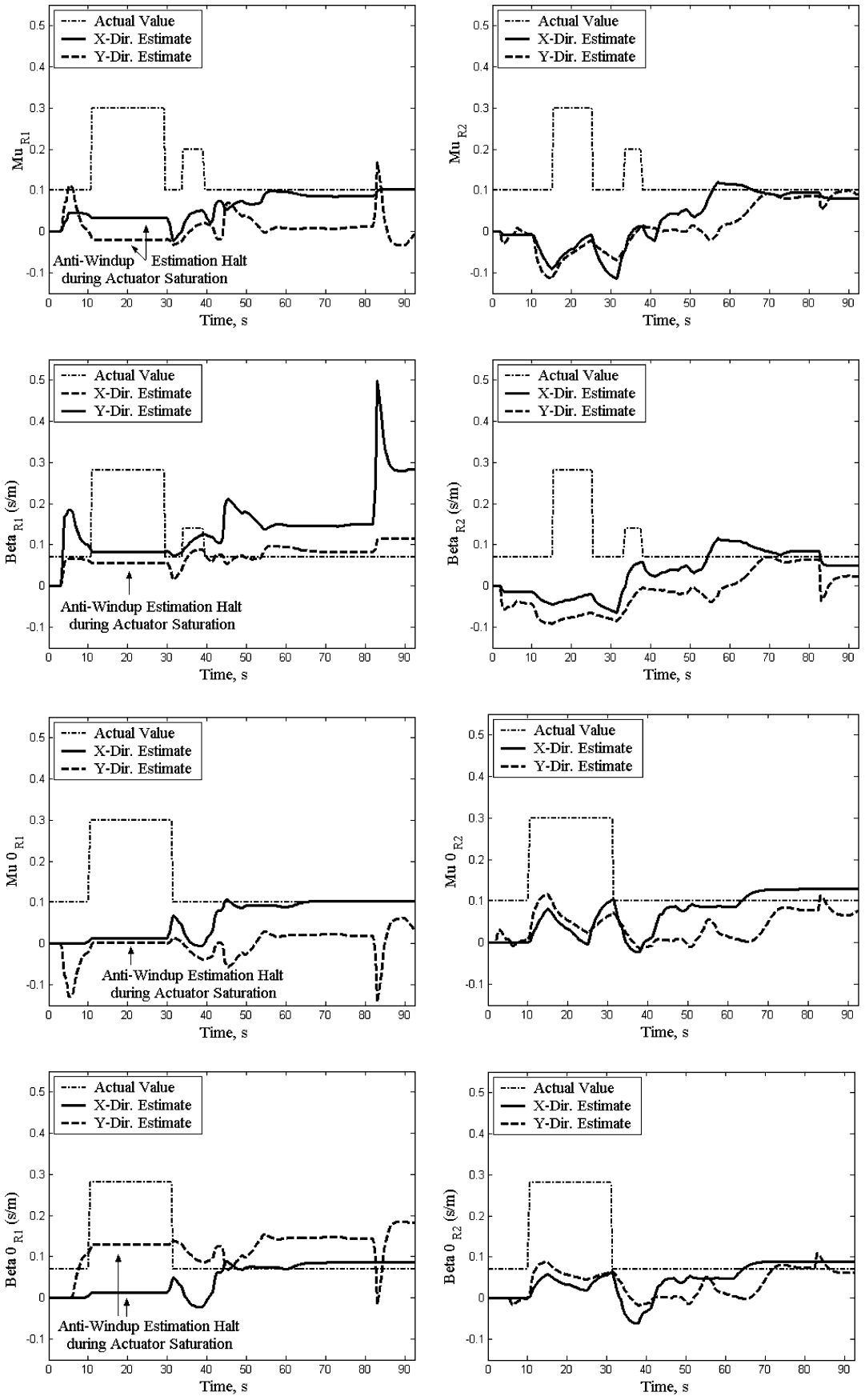

Fig. 6 Estimated and actual frictional parameters along the follower robots' paths. The left column represents follower 1, and the right column represents follower 2.

over unknown terrain on Mars. The results demonstrate 1) formation generation, 2) formation pattern and size change, 3) asymptotic stability of the formation system in nonsaturating conditions, and 4) speed adaptation in the presence of actuator saturation. The simulation parameters used are as follows: masses: $m_0 = 45$ kg, $m_1 = 30$ kg, $m_2 = 15$ kg; saturation limits: $F_0^{\max} = 90$ N, $F_1^{\max} = 45$ N, $F_2^{\max} = 30$ N; friction coefficients: 1) easy terrain: $\mu = 0.1$, $\beta = 0.07$ s $\cdot$ m^{-1}, 2) saturating patch: $\mu = 0.3$, $\beta = 0.28$ s $\cdot$ m^{-1}, 3) difficult patch: $\mu = 0.2$, $\beta = 0.14$ s $\cdot$ m^{-1}; saturation signal delays: $\tau_0 = 0.5$ s, $\tau_1 = 0.5$ s, $\tau_2 = 1$ s; leader's PI controller gains: $k_I = 64\,\text{s}^{-2}$, $k_P = 32\,\text{s}^{-1}$; followers' adaptive controller gains: $k_1 = 36\,\text{s}^{-2}$, $k_2 = 16\,\text{s}^{-2}$, $c_1 = 24\,\text{s}^{-1}$, $c_2 = 16\,\text{s}^{-1}$; followers' adaptive estimator gains: $p_1 = 2.25\,\text{s}^{-1}$, $p_2 = 1\,\text{s}^{-1}$; acceleration due to gravity on Mars: $g = 3.7$ m/s^2.

Figure 2 shows the terrain map, as well as traces and snapshots of the three rovers during a formation navigation mission that lasts nearly 1.5 min. The formation's linear and angular speed commands, which represent the desired speeds of the leader within the formation configuration, are shown in Fig. 3. The percent nondimensional overall formation error is presented in Fig. 4. Rover control-force (magnitude) and linear-speed histories are shown in Fig. 5. Finally, the time histories of frictional-parameter estimates (computed by the follower rovers) and their corresponding true simulation values (traversed terrain's friction coefficients) are shown in Fig. 6. Note that the parameter estimates in the X and Y directions differ from each other as expected and also do not necessarily converge to the terrain's true parameter values. This is due to the fact that our adaptive control scheme does not require (nor guarantee) parameter convergence.

The mission begins with a rendezvous stage, in which the follower robots start off from out-of-formation locations over easy terrain (southwest corner) and rush to get into an initial line-formation configuration with 2.5-m desired spacing, while the leader robot awaits them at rest for about 5 s (Fig. 5). The term "rush" refers to the followers' speed-up period, during which they tend to saturate themselves (favorably) and consequently, the formation tracking error (Fig. 4) undergoes a rapid decay.

Immediately after rendezvous with the line formation facing north, a clockwise synchronized turn (around the southern crater) begins with a desired angular speed of -0.1 rad/s and lasts for 15 s (Fig. 3). The corresponding desired linear speeds are as follows: leader, 1 m/s (as designated by the formation linear speed command in Fig. 3), follower 1, 0.75 m/s, and follower 2, 0.5 m/s (Fig. 5). During this maneuver, the fleet runs into challenging terrain (saturating terrain in Fig. 2), over which follower 1 saturates at 0.375 m/s at time = 10 s (Fig. 5). Upon receiving follower 1's saturation signal, the leader reduces the formation's angular speed to -0.05 rad/s and its own linear speed to 0.5 m/s (Fig. 3) in accordance with the speed adaptation strategy in Eqs. (70) and (71). A small 4% steady-state formation error builds up in the meantime (Fig. 4) and remains until rover 1 exits the patch and unsaturates (time = 30 s). Increased control efforts (without saturating) of the leader and follower 2 over the challenging patch, as a result of their respective PI and adaptive controllers' compensation, can be seen in Fig. 5. Note that as can be seen in Fig. 6, all parameter estimation within follower 1 is halted during the saturation period in order to avoid integral windup and reduce desaturation overshoot.

At time = 20 s, when the formation is headed about 30 deg northeast and still on the challenging terrain, the fleet begins a straight-line cruise. At this time, the formation linear speed command is further lowered to follower 1's saturation speed (0.375 m/s) for straight-line motion until time = 30 s, when rover 1 exits the saturating patch (Fig. 3). For another 10 s, the fleet keeps straight while the followers (leader on easy terrain) cross another difficult patch (Fig. 2). Over this difficult patch, however, both followers are able to keep in formation (zero error) by increasing their control efforts without saturating, and travel at the desired speed of 1 m/s (Fig. 5), thus showing adaptive formation-keeping over unknown and changing terrain.

At time 40 s, the followers are commanded by the leader to switch to column formation through a ladder transition in order to avoid a sand dune (Fig. 2). The followers perform the transition through a rapid slowdown, turning 90 deg left, speeding up across the line formation span, and finally turning 90 deg right to get behind the leader, all while trying to keep their Euclidian distance to the moving leader at their current desired separation values, 2.5 and 5 m (Fig. 5). As can be seen in Fig. 3, some small transient errors occur during the abovementioned transition maneuver. Note that during ladder transition, the formation geometry varies continuously in a desired manner (flexible formation) as compared to that of a rigid formation.

After the transition, starting at about time 50 s, the fleet exhibits convoy motion (Fig. 2) as it goes around the corner of the northern sand dune at a 4-m turning radius with corresponding speeds of 1 m/s and 0.25 rad/s (Fig. 3). In the formation snapshot shown, the leader is moving north on a straight path past the curve, follower 1 is in the middle of the turn tracing the leader's arc path, and follower 2 is still moving straight at 30 deg northeast, tracing the leader's former path (preceding the curve). As can be seen in Fig. 5, during this maneuver, the rovers smoothly maintain their desired formation speed (1 m/s), while the formation error remains nearly zero throughout (Fig. 4).

Past the convoy turn, the fleet travels straight in column formation between the northern sand dune and crater before making a 180-deg turn along a 5-m-radius circular path around the crater (Fig. 2). The snapshot shows the rovers' relative headings along the arc. Past the crater with the formation southbound, the followers switch back to a line formation (Fig. 2) with reduced size of 3 m (1.5-m spacing), following the leader's command at time 80 s. This maneuver, which takes about 8 s to complete, further shows the asymptotic stability and formation control capabilities of our proposed adaptive control scheme (Fig. 4). Note that the error hike corresponds to the positional difference (perceived as error) between the current (column) and desired (line) configurations at the beginning of the transition (time 80 s). Finally, the fleet finishes the navigation, following a stop command at time 90 s (Fig. 3).

VIII. Conclusions

We have developed a novel rover-formation adaptive-control architecture and demonstrated it using two-dimensional simulation of point-mass rovers. We have proved theoretically that our adaptive controllers guarantee that formation error decreases to zero asymptotically under nonsaturated conditions. This does not imply, however, that control parameter estimates corresponding to the actual terrain-friction parameters converge to their true values (nor do we require them to do so). When one or more rovers experience actuator saturation, the entire rover fleet reduces its speed based on that of the slowest saturated robot using a speed adaptation strategy. In this way, the formation error is kept small and bounded during saturation occurrences over difficult terrains. Our simulation results showed that our control architecture can be used to achieve a variety of formation geometries, and enables the formations to move in straight-line or circular trajectories. As shown by the simulation, the architecture can also be used to achieve convoylike train motion of a set of rovers. Furthermore, rover formations can switch from one geometry to another geometry using special transition maneuvers.

There are a number of areas in which this work could be extended. The focus of this work was mainly on group formation adaptive control theory, rather than individual agent vehicle dynamics. Thus, we used simple point-mass models to represent the robots. Work has been undertaken by other researchers to create "holonomic" rovers that can be fully actuated using three holonomic drives, whose translational motion can be controlled independent of their rotational motion. In general, however, the control methodology presented in this paper should be extended/modified to more realistic robot dynamic models for field rover applications.[30]

In this paper, we employed generic terrain-friction parameters that could account for terrain variation. It would be valuable to validate the appropriateness of these terms for specific missions using both advanced terrain simulators, or in mission-simulated hardware field tests. One limitation of our current terrain estimation is that we assume that the terrain is flat. Our architecture can be extended in a straightforward way by including a slope estimator into our controller, at the cost of added controller complexity. As more realistic

rover designs and terrain models are incorporated into this work, the tradeoff between controller complexity and formation performance will be an important area of study.

Acknowledgments

We thank the editors and the anonymous reviewers for their very helpful discussion and comments. The work performed by the third author was carried out at the Jet Propulsion Laboratory, California Institute of Technology, under a contract with the National Aeronautics and Space Administration.

References

[1]Musser, G., "The Spirit of Exploration," *Scientific American*, Vol. 290, No. 3, 2004, pp. 52–57.

[2]Cao, Y., Fukunaga, A., and Kahng, A., "Cooperative Mobile Robotics: Antecedents and Directions," *Autonomous Robots*, Vol. 4, No. 1, 1997, pp. 7–27.

[3]Huntsberger, T. L., Pirjanian, P., Trebi-Ollennu, A., Das, H., Aghazarian, H., Ganino, A., Garrett, M., Joshi, S., and Schenker, P., "CAMPOUT: A Control Architecture for Tightly Coupled Coordination for Multi-Robot Systems for Planetary Surface Exploration," *IEEE Transactions on Systems, Man, and Cybernetics*, Vol. 33, No. 5, 2003, pp. 550–559.

[4]Schenker, P., Huntsberger, T. L., Pirjanian, P., Baumgartner, E., and Tunstel, E., "Planetary Rover Developments Supporting Mars Exploration, Sample Return, and Future Human Robotic Colonization," *Autonomous Robots*, Vol. 14, Nos. 2–3, 2003, pp. 103–126.

[5]Balch, T., and Arkin, R. C., "Behavior Based Formation Control for Multirobot Teams," *IEEE Transactions on Robotics and Automation*, Vol. 14, Dec. 1998, pp. 926–939.

[6]Schneider-Fontan, M., and Mataric, M. J., "Territorial Multirobot Task Division," *IEEE Transactions on Robotics and Automation*, Vol. 14, Oct. 1998, pp. 815–822.

[7]Parker, L., "ALLIANCE: An Architecture for Fault Tolerant Multirobot Cooperation," *IEEE Transactions on Robotics and Automation*, Vol. 14, April 1998, pp. 220–240.

[8]Wang, P. K. C., Hadaegh, F., and Lau, K., "Synchronized Formation Rotation and Attitude Control of Multiple Free Flying Spacecraft," *Journal of Guidance, Control, and Dynamics*, Vol. 22, No. 1, 1999, pp. 28–35.

[9]Mesbahi, M., and Hadaegh, F. Y., "Formation Flying Control of Multiple Spacecraft via Graphs, Matrix Inequalities, and Switching," *Journal of Guidance, Control, and Dynamics*, Vol. 24, No. 2, 2001, pp. 369–377.

[10]Scharf, D., Hadaegh, F., and Ploen, S., "A Survey of Spacecraft Formation Flying Guidance and Control (Part II)," *Proceedings of the American Control Conference*, IEEE Publications, Piscataway, NJ, 2004, pp. 2976–2985.

[11]Giulietti, F., Pollini, L., and Innocenti, M., "Autonomous Formation Flight," *IEEE Control Systems Magazine*, Vol. 20, No. 6, 2000, pp. 34–44.

[12]Stilwell, D., and Bishop, B., "Platoons of Underwater Vehicles," *IEEE Control Systems Magazine*, Vol. 20, No. 6, 2000, pp. 45–52.

[13]Lawton, J. R., Young, B. J., and Beard, R. W., "A Decentralized Approach to Elementary Formation Maneuvers," *IEEE Transactions on Robotics and Automation*, Vol. 19, No. 6, 2003, pp. 933–941.

[14]Lewis, M. A., and Tan, K., "High Precision Formation Control of Mobile Robots Using Virtual Structures," *Autonomous Robots*, Vol. 4, No. 4, 1997, pp. 387–403.

[15]Ren, W., and Beard, R. W., "Formation Feedback Control for Multiple Spacecraft via Virtual Structures," *IEEE Proceedings—Control Theory Applications*, Vol. 151, No. 3, 2004, pp. 357–368.

[16]Young, B. J., Beard, R. W., and Kelsey, J. M., "A Control Scheme for Improving Multi-vehicle Formation Maneuvers," *American Control Conference*, IEEE Publications, Piscataway, NJ, 2001, pp. 704–709.

[17]Wang, P. K. C., "Navigation Strategies for Multiple Autonomous Mobile Robots Moving in Formation," *Journal of Robotic Systems*, Vol. 20, No. 2, 1991, pp. 177–195.

[18]Feddema, J. T., Lewis, C., and Schoenwald, D. A., "Decentralized Control of Cooperative Robotic Vehicles: Theory and Application," *IEEE Transactions on Robotics and Automation*, Vol. 18, No. 5, 2002, pp. 852–864.

[19]Swaroop, D., and Hedrick, J., "String Stability of Interconnected Systems," *IEEE Transactions on Automatic Control*, Vol. 41, No. 3, 1996, pp. 349–357.

[20]De Queiroz, M. S., Kapila, V., and Yan, Q., "Adaptive Nonlinear Control of Multiple Spacecraft Formation Flying," *Journal of Guidance, Control, and Dynamics*, Vol. 23, No. 3, 2000, pp. 385–390.

[21]Lawton, J., Beard, R., and Hadaegh, F., "An Adaptive Control Approach to Satellite Formation Flying with Relative Distance Constraints," *Proceedings of the IEEE American Controls Conference*, IEEE Publications, Piscataway, NJ, 1999, pp. 1545–1549.

[22]Singh, S., Zhang, R., Chandler, P., and Banda, S., "Decentralized Adaptive Close Formation Control of UAV's," AIAA Paper 2001-0106, 2001.

[23]Swaroop, D., Hedrick, J., and Choi, S., "Direct Adaptive Longitudinal Control of Vehicle Platoons," *IEEE Transactions on Vehicular Technology*, Vol. 50, No. 1, 2001, pp. 150–161.

[24]Joshi, S. S., "Multilevel Adaptation for Autonomous Mobile Robot Formations," AIAA Paper 2000-4167, Aug. 2000.

[25]Joshi, S. S., Riehl, J. R., and Ganji, F., "Investigation of Target-Speed Adjustment of the Lead Robot in an Adaptively Controlled Multiple-Robot Formation," AIAA Paper 2002-4563, Aug. 2002.

[26]Ganji, F., Joshi, S. S., and Bayard, D. S., "Adaptive Rover Formation Control over Unknown Terrains," AIAA Paper 2005-6463, Aug. 2005.

[27]Lucas, G. G., *Road Vehicle Performance: Methods of Measurement and Calculation*, Gordan & Breach, New York, 1986.

[28]Iagnemma, K., Kang, S., and Dubowsky, S., "Online Terrain Parameter Estimation for Wheeled Mobile Robots with Application to Planetary Rovers," *IEEE Transactions on Robotics*, Vol. 20, No. 5, 2004, pp. 921–927.

[29]Ji, M., Zhang, Z., Biswas, G., and Sarkar, N., "Hybrid Fault Adaptive Control of a Wheeled Mobile Robot," *IEEE/ASME Transactions on Mechatronics*, Vol. 8, No. 2, 2003, pp. 226–233.

[30]Ganji, F., "Adaptive Formation Control for Planetary Exploration Rovers," Ph.D. Dissertation, Dept. of Mechanical and Aeronautical Engineering, Univ. of California, Davis (unpublished).

[31]Slotine, J. J., and Li, W., *Applied Nonlinear Control*, Prentice–Hall, Englewood Cliffs, NJ, 1991.